Very high resolution measurement of the penetration depth of superconductors by a novel single-coil inductance technique

A. Gauzzi[a)]
Laboratoire de Physique du Solide, ESPCI, 75231 Paris, France and MASPEC, Consiglio Nazionale delle Ricerche, 43010 Parma, Italy

J. Le Cochec and G. Lamura
Laboratoire de Physique du Solide, ESPCI, 75231 Paris, France

B. J. Jönsson[b)] and V. A. Gasparov[c)]
Département de Physique, Ecole Polytechnique Fédérale (EPFL), 1015 Lausanne, Switzerland

F. R. Ladan and B. Plaçais
LPMC de l'ENS, UMR 8551 associé au CNRS et aux Universités Paris 6 et 7, 75231 Paris Cedex 5, France

P. A. Probst
Scientific Consulting, 1603 Grandvaux, Switzerland

D. Pavuna
Département de Physique, Ecole Polytechnique Fédérale (EPFL), 1015 Lausanne, Switzerland

J. Bok
Laboratoire de Physique du Solide, ESPCI, 75231 Paris, France

(Received 3 August 1999; accepted for publication 20 January 2000)

We describe a novel single-coil mutual inductance technique for measuring the magnetic penetration depth λ of superconductors at 2–4 MHz as a function of temperature in the 4–100 K range. We combine a single-coil configuration with a high-stability marginal oscillator; this enables us to measure the absolute value of λ on both bulk samples and thin films with very high resolution ($\delta\lambda = 10$ pm) and a precision of 30 nm. As example of application, we report measurements on NbTi bulk samples and Nb films. This contactless technique is suited for probing the superconducting properties of samples over large surfaces. © *2000 American Institute of Physics*. [S0034-6748(00)02505-3]

I. INTRODUCTION

The low-energy excitation spectrum of a superconductor determines all thermodynamic and electrodynamic properties of the superconducting state. The precise knowledge of this spectrum is required to evaluate the performances of applications like superconducting quantum interference devices (SQUIDs), filters, fault current limiters, magnets, etc. Furthermore, the symmetry of the excitation spectrum gives insight into the nature of the effective interaction responsible for the superconducting transition. In this respect, the experimental evidence for unconventional (or non-*s*) symmetry, such as *p*- or *d*-like, reported on most compounds of heavy fermions,[1] cuprates,[2,3] and rhutenates[4,5] has attracted a great interest. However, most data, such as those based on SQUID experiments on cuprates,[3] are not conclusive or in contrast with other data.[6] Such discrepancy may be due to the extreme sensitivity of the spectrum to impurities or second-order interactions that are not responsible for the pairing mechanism.[7] More systematic studies and more sensitive techniques are therefore needed to elucidate the nature of the superconducting state of complex materials.

Here we consider those experimental methods enabling the determination of the low-energy excitation spectrum of superconductors from measurements of the imaginary part of the complex conductivity $i\sigma''_\omega$ at a given angular frequency ω. From this quantity we can determine the magnetic penetration depth λ, which is related to the superfluid density n_S. Two regions of temperatures are of interest: (1) in the vicinity of the transition temperature T_c, σ'' provide information on the critical behavior of the superconducting order parameter; (2) at low temperatures, $T \approx 0$, the temperature dependence of λ reflects the size and symmetry of the superconducting gap function $\Delta_{\mathbf{k}}$. In bulk samples and single crystals, λ is usually measured by using techniques based on cavity or muon-spin rotation techniques. The former technique is applicable to films if the sample can be mounted as an end plate to a host cavity.[8] This setup requires films with a well-defined shape prepared on substrates with low dielectric losses at microwave frequencies. Due to these limitations, superconducting films are commonly measured by the two-coil mutual inductance technique pioneered by Hebard and Fiory[9] and later modified by other authors.[10,11] This technique has the advantage of being nondestructive and contact-

a)Author to whom correspondence should be addressed; electronic mail: gauzzi@maspec.bo.cnr.it
b)Present address: Department of Physics, University of California, San Diego, La Jolla, CA 92093-0319.
c)Permanent address: Institute of Solid State Physics, Russian Academy of Sciences, Chernogolovka 142432, Russian Federation.

less, but is suited only for samples with a well-defined thickness.

Here we describe a novel single-coil inductance technique enabling us to measure the absolute value of λ with very high resolution on any bulk or thin film samples, provided a flat surface of a few mm^2 is available. The single coil geometry, originally proposed by Gasparov and Oganesyan,[12] has the same advantages of the two-coil geometry and provides two additional advantages: (1) a better control of the sample-coil arrangement, implying an easier calibration for measuring the absolute value of λ, as discussed later; (2) a higher sensitivity to the variations of λ. Thanks to (2), it was possible to observe the Kosterlitz–Thouless–Berzinskii vortex–antivortex unbinding transition in ultrathin YBaCuO films.[13] The new setup of the single-coil technique presented here combines the simplicity of the single-coil configuration with the high frequency stability (~0.2 Hz) of a specially designed marginal oscillator (see Ref. 14 and Fig. 1). Thanks to this arrangement, the resolution in the measurement of λ has been further enhanced and is now in the 10 pm range.

This article is organized as follows: (i) we summarize the basic principle of operation of the experimental technique (Sec. II); (ii) we outline the inversion procedure used to convert the raw data into data of λ and recall the basic equations of electrodynamics of superconductors (Sec. III). A review on these equations is given elsewhere;[8] (iii) we describe the experimental setup adopted (Sec IV); (iv) as example of application, we report measurements on reference NbTi bulk samples and Nb films (Sec. V).

II. PRINCIPLE OF OPERATION

The single-coil inductance technique described here is based on the same principle as reported elsewhere.[12,13] λ is measured as a change of impedance ΔZ of a pancake coil located in the proximity of the sample and connected in parallel with a low-loss capacitor. The bridge method used previously[12,13] for measuring ΔZ has limited frequency resolution due to the typically low Q value of the resonant LC circuit [we recall that $Q^{-1}=R/\omega L$, see also Eq. (1)]. We have significantly enhanced this resolution by connecting the above LC circuit at the input of a marginal oscillator (see Figs. 1 and 2). The principle of operation of this device is described in detail elsewhere;[14] in summary, a change of impedance of the LC circuit is detected as a change of resonant frequency f and amplitude V of the oscillating signal. The LC parameters are chosen to set f at 2–4 MHz, which is within the range of optimum operation of the oscillator. Without sample, these parameters fall in the 2–8 μH and 0.5–1 nF range, respectively. The very high sensitivity of the method arises from the strong mutual inductance between sample and coil in the single-coil geometry, in addition to the very high frequency stability of the oscillator. The successful application of the above principle of operation requires:

(1) an adequate procedure for converting the raw f and V data into data of λ. This procedure is an inversion procedure, since λ appears in implicit form in the final Eq. (9);

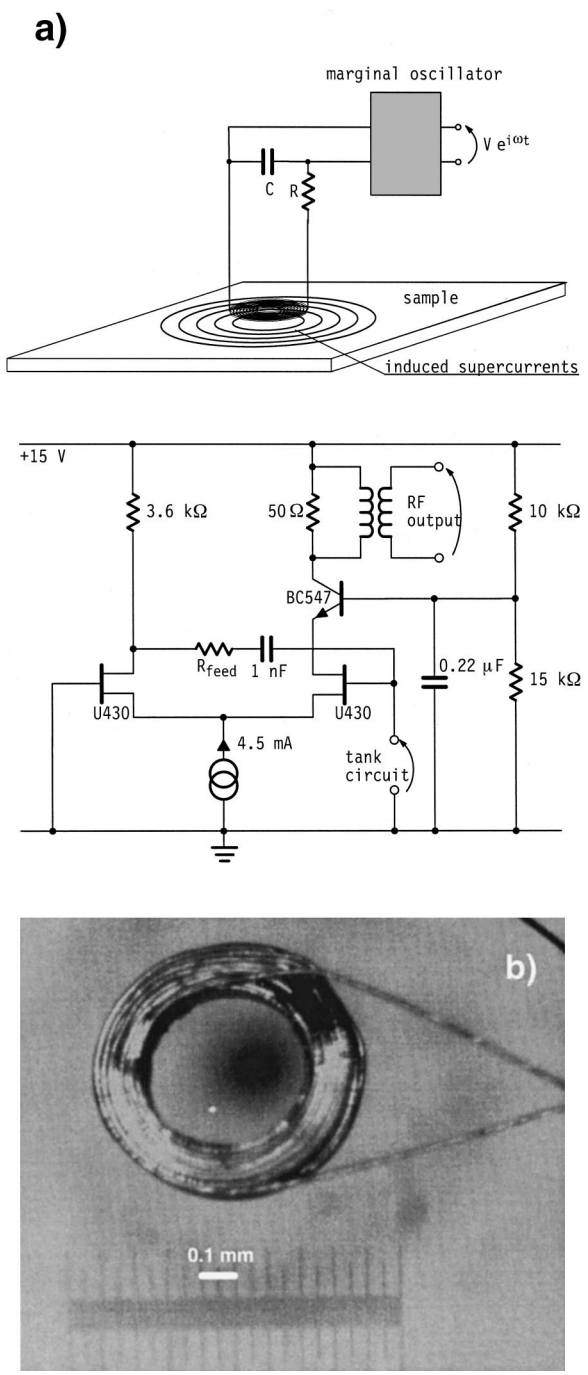

FIG. 1. (a) Top panel: block diagram of the experimental setup showing the coil–sample arrangement, the LC circuit, and the marginal oscillator. Bottom: schematic circuit of the oscillator; see Ref. 14 for further details. (b) Magnified photograph of a miniaturized coil mounted in the setup.

(2) any temperature-dependent changes of impedance detected by the oscillator must only arise from a change of conductivity of the sample. Thus, we must prevent any parameter of the circuit, except the sample, from changing with temperature.

The above two points are discussed in Secs. III and IV.

III. BASIC EQUATIONS: INVERSION PROCEDURE

This procedure consists of two steps. First, the raw data of frequency f and amplitude V of the oscillation are trans-

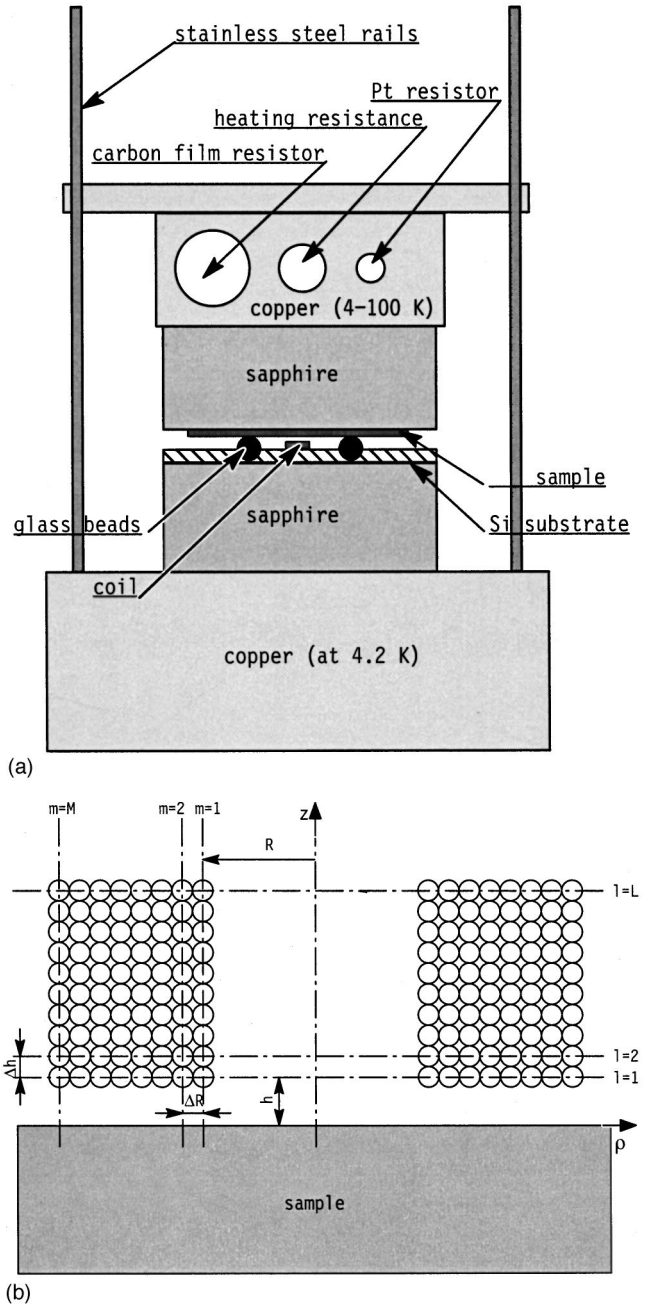

FIG. 2. (a) Cross-sectional view of the sample holder and coil arrangement. (b) Detailed cross-sectional view of the coil–sample arrangement showing the relevant distances. Notations are as in the Appendix.

formed into data of impedance Z_ω of the coil. Second, the Z_ω values are converted into values of σ_ω of the sample. As to the first step, the resonant circuit of Fig. 1 is characterized by the following resonant frequency $f \equiv \omega/2\pi$:

$$f(T) = \frac{1}{2\pi}\sqrt{\frac{1}{L(T)C} - \left[\frac{R(T)}{L(T)}\right]^2}, \tag{1}$$

where C is the capacitance and L and R are, respectively, the inductance and resistance of the coil coupled to the sample. In Eq. (1) we emphasize that C is temperature independent, since the capacitor is kept at 4.2 K while L and R both vary with temperature, since they depend on sample conductivity. The dependence of V_ω on Z_ω is obtained from the nonlinear $(I–V)$ characteristic of the oscillator[14]

$$V(T) = \beta\sqrt{\alpha - \frac{R(T)C}{L(T)}}, \tag{2}$$

where α and β are two characteristic parameters of the oscillator. By inverting the system formed by Eqs. (1) and (2), the impedance $Z_\omega \equiv R_\omega + i\omega L$ of the coil can be extracted from the raw f and V data. Here we limit our discussion to the variations of L (and hence of λ). The reason is twofold. First, we focus our attention on the low-temperature region where dissipation phenomena are usually negligible. Second, a quantitative study of the above phenomena would require a modification of our experimental setup according to the following considerations. From Eq. (1) it follows that the frequency change Δf induced by a change of inductance ΔL or resistance ΔR is $2\Delta f/f = \Delta L/L$ or $\Delta f/f^3 = 4\pi^2 C^2 R \Delta R$, respectively. By taking into account the above typical values for L and C and that $R = 0.2\ \Omega$ without sample, we conclude that the resolution δL and δR of a 0.2 Hz resolution measurement is 100 fH and 5 mΩ, respectively. In our arrangement frequency measurements are therefore sensitive to tiny variations of L but less sensitive to variations of R. Loss measurements by measuring frequency changes are possible if ΔR is large enough, i.e., in the normal state or in the superconducting state sufficiently near the transition.[15] This case is not treated here. Sample-induced changes of resistance could be more easily measured as a change of the oscillation amplitude V_ω [see Eq. (2)]. However, the calibration of the $I–V$ characteristics of the oscillator, which determines the parameters α and β, would require a modification of the circuit to achieve the necessary thermal stability.

The second step of the inversion procedure requires solving Maxwell's equations in the coil-sample geometry [see Fig. 2(b)]. The sample is modeled as an infinite slab of thickness d. This approximation neglects finite-size effects, which is correct if the coil dimension is much smaller than the sample dimension. Numerical simulations indicate that this condition is fulfilled in samples larger than $\approx$4 mm. By explicitly separating the current density in the coil $\mathbf{j}_{\omega,\mathrm{coil}}$ from that of the sample $\mathbf{j}_{\omega,\mathrm{sample}}$ we write in the London gauge $(\mathrm{div}\,\mathbf{A} = 0)$

$$\nabla^2 \mathbf{A}_\omega = -\mu_0(\mathbf{j}_{\omega,\mathrm{coil}} + \mathbf{j}_{\omega,\mathrm{sample}}). \tag{3}$$

We consider the case of low frequencies within the limit of validity of Ohm's law; we then write

$$\mathbf{j}_{\omega,\mathrm{sample}} = i\omega\sigma_\omega \mathbf{A}_\omega. \tag{4}$$

The validity of the local Ohm's law implies one-mode electrodynamics; this restricts the validity of the analysis to the vortex-free states (Meissner and normal states). As recently shown,[16] the presence of vortices entails a two-mode electrodynamics, respectively associated with vortex line tension and viscous drag. This significantly affects both the inductive and resistive linear response of a superconductor. By inserting Eq. (4) into Eq. (3), the solution for the field $\mathbf{A}_\omega$ becomes a function of $\mathbf{j}_{\omega,\mathrm{coil}}$ and σ_ω, where the latter is the only free parameter. The former is a known function, pro-

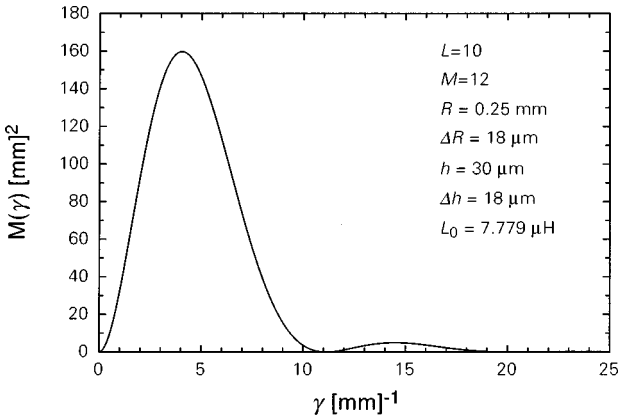

FIG. 3. Plot of the $M(\gamma)$ function [see Eq. (6)] for a coil–sample distance $h=30$ μm. Notations are as in the Appendix.

vided that the geometry of the current distribution in the coil and the distance of the coil–sample is known (see the Appendix). The perturbation of the field produced by the sample is detected as a change of coil impedance Z_ω. By definition

$$I_\omega Z_\omega = i\omega \oint \mathbf{A}_\omega \, d\mathbf{l}, \tag{5}$$

where I_ω is the current flowing through the coil and the path integral is calculated along the spiral forming the coil. The wire forming the latter is modeled as if it were infinitely thin; this approximation is valid because the wire diameter is much thinner than the skin depth at the working frequency. In this case, following the formalism proposed by Pearl,[17] the explicit dependence of Z_ω on σ_ω can be calculated *exactly*. The result is the following (see the Appendix for more details on the algebra):

$$Z_\omega = Z_{0,\omega} - i\pi\omega\mu_0 \int_0^\infty \frac{M(\gamma)}{1+2\gamma l \coth\dfrac{d}{l}} d\gamma, \tag{6}$$

where $Z_{0,\omega}$ is the value of Z_ω without sample and is calculated separately only once. $M(\gamma)$ depends only on the coil geometry and coil–sample distance h (see Ref. 11, Fig. 2 and the Appendix), γ is a wave number in the xy plane, and l is a complex length defined as

$$l \equiv \sqrt{\frac{i}{\omega\mu_0\sigma_\omega}}. \tag{7}$$

This distance is reduced to the London penetration depth for superconductors in the London regime considered here [see Eqs. (8) and (9)]. $M(\gamma)$ plays the role of mutual inductance between coil and sample at a given wave number γ. The range of values $\overline{\gamma}$ giving the dominant contribution to $M(\gamma)$ is on the order of the inverse of the internal diameter of the coil. In our case, $\overline{\gamma} \sim 4\times 10^3$ m^{-1}, as it appears from the numerical example given in Fig. 3.

Thanks to Eq. (6), in principle we can measure the complex conductivity of any sample (superconducting or not) by measuring the variation $\Delta Z_\omega \equiv Z_\omega - Z_{0,\omega}$ of coil impedance. Here we consider only the specific case of a superconducting sample in the London regime, which is valid sufficiently far from T_c. The effects of vortex states are negligible in the linear regime at sufficiently low coil currents. For currents producing magnetic fields below 10^{-4} T in proximity of the sample, which is our case, the frequency is found to be independent from the amplitude. The electromagnetic response of the sample is then mostly diamagnetic and losses are negligible. The explicit expression of the complex conductivity becomes

$$\begin{cases} \sigma''_\omega = \dfrac{1}{\omega\mu_0\lambda^2} \\ \sigma'_\omega \approx 0 \quad (\omega \neq 0, \ \hbar\omega \ll \Delta). \end{cases} \tag{8}$$

By replacing the above expression into Eqs. (6) and (7), we obtain the final expression for the variation of coil inductance

$$L = L_0 - \pi\mu_0 \int_0^\infty \frac{M(\gamma)}{1+2\gamma\lambda \coth\dfrac{d}{\lambda}} d\gamma. \tag{9}$$

In summary, when the coil is placed close to the superconducting sample as shown in Fig. 2, in the London regime, mainly the inductive part of the coil impedance is changed. This change is detected as a change of frequency f and converted into variation of λ thanks to Eq. (9).

IV. EXPERIMENTAL SETUP

A schematic diagram is shown in Figs. 1 and 2. The core of the setup is a precision miniaturized pancake coil made of a 18 μm diam copper wire. The internal and external coil diameters are 0.5 and 0.8–0.9 mm, respectively, depending on the number of turns [see Fig. 1(b)]. Typically, the winding consists of 9–11 sheets of 8–10 turns each. As previously mentioned, the resulting self-inductance L_0 falls in the 2–8 μH range. The capacitor is a low-loss monolithic multilayer ceramic chip of 0.5–1 nF with very high temperature stability.

The coil–sample arrangement has been designed to satisfy two requirements:

(1) to control the sample–coil distance h as much as possible to precisely measure the absolute value of λ. Indeed, from Eqs. (9) and (A3) it follows that an uncertainty δh in the measure of h produces an uncertainty $\delta\lambda \approx \delta h/2h\overline{\gamma}$ for bulk samples. For thin films, in the above expression, λ must be replaced by the effective penetration depth $\lambda \coth(d/\lambda)$. Similar considerations are extensively discussed in Refs. 18 and 19 for the two-coil geometry, where the relative position of the second (pickup) coil with respect to the first (drive) coil constitutes an additional parameter to be controlled for achieving the desired precision and resolution of the measurement.

(2) To minimize heat conduction between sample and coil. This is necessary to prevent any temperature-induced changes of coil resistance, since the oscillator is sensitive to every tiny change of impedance in any points of the input circuit. So, while changing the sample temperature, the coil and the other parts of the circuit must be kept at constant temperature.

In order to fulfill both conditions, we have thermally isolated the sample from the coil by positioning three ≈0.5 mm diam SiO_2 beads between the sapphire block supporting the coil and the sample surface [see Fig. 2(a)]. The resulting coil–sample spacing is ≈0.1 mm. This distance is precisely estimated by measuring a reference sample with a known value of λ. The heat conduction between sample and coil is negligible thanks to the low residual helium pressure inside the cryostat ($<10^{-6}$ Torr). To avoid any temperature variation of circuit parameters, the coil and capacitance are thermalized by a copper heat sink at 4.2 K. The coil is placed onto a sapphire block to avoid the induction of parasitic currents and ensure best thermal contact with the heat sink. The sample is thermalized by a copper sample holder.

In summary, heat conduction between sample and coil is minimized thanks to the modest thermal conductivity of glass and the tiny surface of the beads in contact with the coil holder. The effectiveness of this arrangement to keep all objects, except the sample, at constant temperature is confirmed by the negligible background signal obtained without sample. The drift signal arising from the electronic circuit is minimized by regulating the temperature of the circuit at a value slightly larger than room temperature.

As for the control of the sample–coil distance h, our measurements of frequency changes without sample indicate that h is not affected by thermal expansion effects of the glass beads. Indeed, if the latter were significantly heated by the sample, their expansion would be <5 nm below 50 K and <20 nm below 100 K thanks to the small thermal expansion coefficient of glass.[20] Such variations would correspond to frequency variations ~ -0.1 Hz/nm. The observed variations are within the stability level of the oscillator at temperatures below 100 K, so we conclude that thermal expansion effects are within the experimental resolution below 100 K. Other sources of systematic errors in the measurement of λ are the imperfect parallelism between sample and coil and the precision of the coil impedance measurement. Ultimately, the latter turns out to be the dominant factor limiting the precision of our measurements of λ; in the present arrangement we estimate this precision to be ~30 nm. On the other hand, the very high stability of the oscillator, in addition to negligible background signal and heat expansion effects, enables us to achieve a very high resolution $\delta\lambda$. From Eq. (9) and Fig. 3 and by recalling that $\delta L \approx 100$ fH, we obtain $\delta\lambda \approx 10$ pm.

V. APPLICATION TO NbTi AND Nb SAMPLES

In Figs. 4(a) and 4(b) we report the raw amplitude and frequency data obtained on a standard NbTi bulk sample and a 120 nm thick Nb film prepared on (111) Si by magnetron sputtering. These two materials are taken as reference to test the reliability of the technique, since it has been reported on both[21,22] that the temperature dependence of λ follows the Bardeen–Cooper–Schrieffer (BCS) prediction for conventional superconductors with a nearly isotropic *s*-wave gap. This prediction is obtained by assuming the BCS energy spectrum $\epsilon_{\mathbf{k}}$ in the usual Fermi liquid-like expression for the normal fraction of the total electron density ρ (Ref. 23)

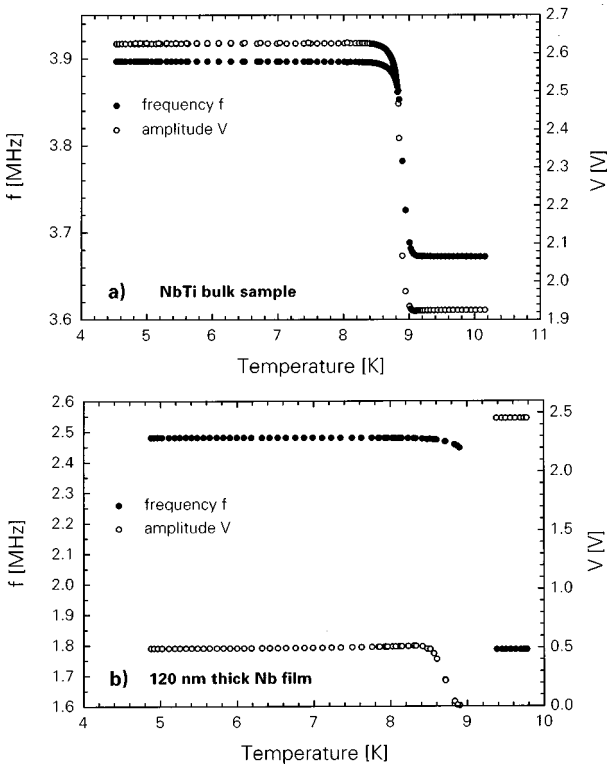

FIG. 4. Example of application of the technique to a NbTi bulk sample (a) and a 120 nm thick Nb film prepared on Si by magnetron sputtering (b). For both samples, the raw frequency f and oscillation amplitude V data are plotted as a function of temperature. In (b), the missing data in the transition region are due to the decrease of the Q value of the oscillator below the threshold value enabling the oscillation [see Eqs. (1) and (2)].

$$x_n = 1 - \left[\frac{\lambda(0)}{\lambda(T)}\right]^2 = -\frac{2}{3}\frac{\hbar^2}{\rho}\int k^2 \frac{\partial f(\epsilon_{\mathbf{k}})}{\partial \epsilon_{\mathbf{k}}} \frac{d^3k}{(2\pi)^3}, \qquad (10)$$

where f is the Fermi distribution function. At sufficiently low temperatures, Eq. (10) tend to the well-known exponential form $\lambda(T)-\lambda(0) \propto \exp(-\Delta/k_B T)$, which has been experimentally confirmed in other BCS-type superconductors, such as NbCN films.[18]

From Figs. 4(a) and 4(b) we note the following: (1) the superconducting transition manifests itself as a jump of the resonant frequency f; this corresponds to the screening effect of the supercurrents in the sample that reduce the coil inductance [see Eq. (1)]. The transition temperatures are 8.9 and 9.1 K for the NbTi and Nb samples, respectively; both values are in the range of values reported in the literature.[21,22,24] The transition begins just before the end of the tail of the resistive transition; (2) across the transition, the amplitude V of the oscillating signal is influenced by two factors with opposite effects [see Eq. (2)]: V tends to increase because of the drop of sample resistance and to decrease because of the drop of coil inductance. The first effect dominates in samples with thickness larger than the skin depth, as our NbTi bulk samples, where the absorption of the electromagnetic field is large in the normal state. The increase of dissipation in the transition region is usually small in these samples and hardly visible as a dip of amplitude. As a result, a jump of amplitude similar to that of frequency is observed in the temperature dependence. In thin films, as our Nb films, the absorp-

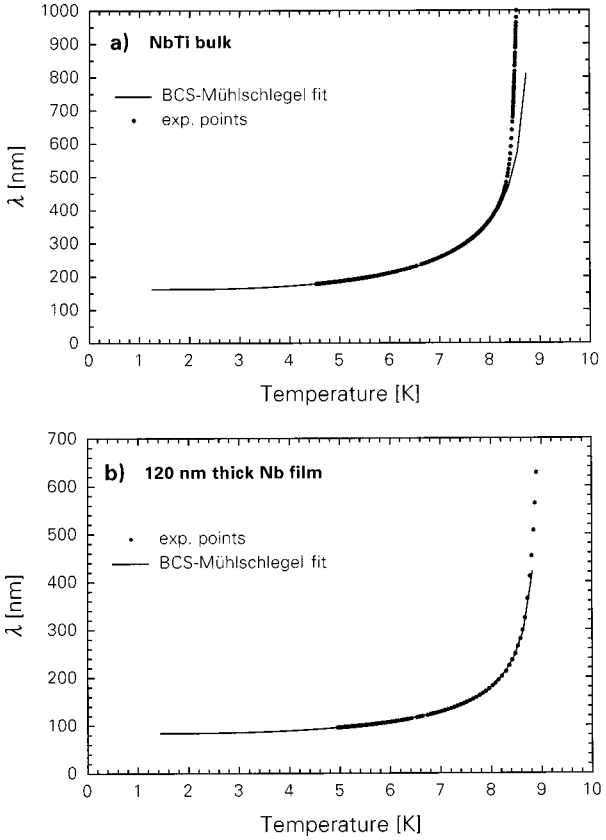

FIG. 5. Conversion of the raw data of Fig. 4 into λ data by using the conversion formula Eqs. (1), (2), and (9). The solid line represents a fit of the data by using the BCS prediction [Eq. (10)] for conventional *s*-wave weak-coupling superconductors. For the NbTi sample, the deviation of the data from the above prediction near the transition is discussed in the text.

tion of the field is negligible in the normal state. In this case the amplitude variations are mainly determined by the drop of coil inductance and the amplitude at low temperatures is smaller than at high temperatures. As a result the above dip becomes pronounced. Below a given threshold value of quality factor Q, no oscillation is possible [see Eqs. (1) and (2)], which is indeed the case of the Nb film in Fig. 4(b).

In Figs. 5(a) and 5(b) we reported the same raw data converted into λ data by using Eqs. (1), (2), and (9). As to the temperature dependence of these data, we find an excellent agreement with Eq. (10) by assuming a conventional isotropic BCS spectrum. In the latter, we have incorporated the exact temperature dependence of the gap by using Mühlschlegel's table.[25] The fit of the experimental data enables us to determine the zero-temperature value of λ. We obtain 163 and 84±30 nm for the NbTi and Nb samples, respectively. These values as well fall within the range reported in the literature.[21,22,24] In the case of Nb, for example, the reported values vary from 43 to 120 nm depending on the degree of sample purity.[24] Indeed, we recall that we measure an *effective* magnetic penetration depth λ. In presence of impurities and disorder, λ is usually larger than the London penetration depth by a factor $\sqrt{1+\xi_0/l}$, where ξ_0 and l are, respectively, the BCS zero-temperature superconducting coherence length and the mean free path of the charge carriers.[8]

As to the temperature dependence of λ near the transition point, an appreciable deviation from the BCS theoretical prediction is observed only in the NbTi sample. The breakdown of the London regime is indeed expected in this temperature region because of dissipative phenomena produced by vortex dynamics, for example.[16] It has been known for many years that these phenomena are more relevant in alloys, such as NbTi, than in pure metal, such as Nb. This is consistent with our experimental result that no appreciable deviation from the BCS prediction is found in our Nb film at any temperature. In conclusion, the above comparison of our data with published data obtained by using various techniques indicates the reliability of the single–coil technique presented here.

ACKNOWLEDGMENTS

The authors acknowledge J.-P. Contour and M. Drouet for their help and encouragement during the early stage of the present work, F. Ferrer and B. Barrau for their help in developing the numerical inversion procedure, and N. Bontemps for a critical reading of the manuscript. They acknowledge Europa Metalli spa-Superconductor Division for kindly providing them with the NbTi sample. A.G. gratefully acknowledges financial support from the European Commission under Contract No. CHRX-CT93-0325.

APPENDIX

To solve Eq. (3), we note that the current density distribution $\mathbf{j}_{\rm coil}$ in the coil lies in the (xy) plane of the sample. Therefore, there is no net current flowing along the perpendicular (z) direction. For simplicity, we consider a sample with isotropic conductivity σ in the plane to avoid complication in the formulas. By rewriting Eq. (3) in cylindrical coordinates, only the orthoradial component A_ϑ of the vector potential $\mathbf{A}$ is nonzero and we obtain

$$\nabla^2 A_\vartheta(\rho,z) = -\mu_0[j_{\vartheta,\rm coil}(\rho,z) + i\omega\sigma H_d(-z)A_\vartheta(\rho,z)], \tag{A1}$$

where the origin and direction of the z axis are chosen as shown in Fig. 2(b), the ω subscripts have been omitted, $H_d(z)$ is the Heaviside function, whose value is unity in the $[0,d]$ interval and zero elsewhere, and d is the thickness of the sample. The current density distribution in the coil formed by L sheets and M turns in the same sheet is modeled as follows:

$$j_{\vartheta,\rm coil} = I\sum_{l=0}^{L-1}\delta(z-h-l\Delta h)\sum_{m=0}^{M-1}\delta(\rho-R-m\Delta R), \tag{A2}$$

where I is the current flowing in the coil, δ is the delta distribution, h is the sample–coil distance, R is the internal coil radius, and Δh and ΔR are the spacings between adjacent sheets and adjacent turns, respectively, in the same sheet [see also Fig. 2(b)].

Following Pearl,[17] Eq. (A1) can be solved exactly. The result is Eq. (6) where the explicit expression for the function $M(\gamma)$ of mutual inductance is reported below

$$M(\gamma)=\left\{ e^{-h\gamma}\sum_{l=0}^{L-1} e^{-l\Delta h\gamma}\sum_{m=0}^{M-1} J_1[\gamma(R+m\Delta R)] \times(R+m\Delta R)\right\}^2, \tag{A3}$$

where γ is a wave number and J_1 is the first order Bessel function. In Fig. 3 we report a plot of $M(\gamma)$ for typical parameters of our experimental setup.

[1] See, for example, F. Gross, B. S. Chandrasekhar, D. Einzel, K. Andres, P. J. Hirschfeld, H. R. Ott, J. Beuers, Z. Fisk, and J. L. Smith, Z. Phys. B: Condens. Matter **64**, 175 (1988).
[2] W. N. Hardy, D. A. Bonn, D. C. Morgan, R. Liang, and K. Zhang, Phys. Rev. Lett. **70**, 3999 (1993).
[3] J. R. Kirtley, C. C. Tsuei, M. Rupp, J. Z. Sun, L. S. Yu-Jahnes, A. Gupta, M. B. Ketchen, K. A. Moler, and M. Bhushan, Phys. Rev. Lett. **76**, 1336 (1996), and references therein.
[4] T. M. Riseman *et al.*, Nature (London) **396**, 242 (1998).
[5] A. P. Mackenzie, R. K. W. Haselwimmer, A. W. Tyler, G. G. Lonzarich, Y. Mori, S. Nishizaki, and Y. Maeno, Phys. Rev. Lett. **80**, 161 (1998).
[6] Li Qiang, Y. N. Tsay, M. Suenaga, R. A. Klemm, G. D. Cu, and N. Koshizuka, Phys. Rev. Lett. **83**, 4160 (1999), and references therein.
[7] A. I. Larkin and Yu. N. Ovchinnikov, Sov. Phys. JETP **20**, 762 (1965); P. Fulde and R. A. Ferrell, Phys. Rev. **135**, 550 (1965); A W. Overhauser and L. L. Daemen, Phys. Rev. Lett. **61**, 1885 (1988); A. Gauzzi and J. Bok, J. Supercond. **9**, 523 (1996).
[8] N. Klein, H. Chaloupka, G. Müller, S. Orbach, H. Piel, B. Roas, L. Schultz, U. Klein, and M. Peiniger, J. Appl. Phys. **67**, 6940 (1990).
[9] A. F. Hebard and A. T. Fiory, Phys. Rev. Lett. **44**, 291 (1980).
[10] A. T. Fiory, A. F. Hebard, P. M. Mankiewich, and R. E. Howard, Appl. Phys. Lett. **52**, 2165 (1988).
[11] B. Jeanneret, J. L. Gavilano, G. A. Racine, Ch. Leemann, and P. Martinoli, Appl. Phys. Lett. **55**, 2336 (1989).
[12] V. A. Gasparov and A. P. Oganesyan, Physica C **178**, 445 (1991).
[13] V. A. Gasparov, I. Batov, Qi Li, and C. Kwon, Physica B (in press); V. A. Gasparov, I. Batov, Qi Li, and C. Kwon, Proc. SPIE **2697**, 391 (1996).
[14] P.-A. Probst, B. Collet, and W. M. MacInnes, Rev. Sci. Instrum. **47**, 1522 (1976).
[15] V. A. Gasparov, M. R. Mkrtchyan, M. A. Obolensky, and A. V. Bondarenko, Physica C **231**, 197 (1994).
[16] B. Plaçais, P. Mathieu, Y. Simon, E. B. Sonin, and K. B. Traito, Phys. Rev. B **54**, 13083 (1996).
[17] J. Pearl, Ph.D. thesis, Polytechnic Institute of Brooklyn, New York, 1965.
[18] J. H. Claassen, M. L. Wilson, J. M. Byers, and S. Adrian, J. Appl. Phys. **82**, 3028 (1997).
[19] S. J. Turneaure, E. R. Ulm, and T. R. Lemberger, J. Appl. Phys. **79**, 4221 (1996).
[20] G. White, in *Experimental Techniques in Low Temperature Physics* (Oxford University Press, Oxford, 1987).
[21] J. Lammer and L. Rinderer, Helv. Phys. Acta **48**, 520 (1975).
[22] L. V. Mercaldo, S. M. Anlage, and L. Maritato, Phys Rev. B **59**, 4455 (1999).
[23] L. D. Landau and E. M. Lifshitz, *Statistical Physics*, Part II (Pergamon, Oxford, 1980).
[24] H. Zhang, J. W. Lynn, C. F. Majkrzak, S. K. Satija, J. H. Kang, and X. D. Wu, Phys. Rev. B **52**, 10395 (1998).
[25] B. Mühlschlegel, Z. Phys. **155**, 313 (1959).